

DECENTRALIZED WIRELESS SENSING AND CONTROL OF CIVIL STRUCTURES

Yang Wang ^a, R. Andrew Swartz ^b, Jerome P. Lynch ^b, Kincho H. Law ^a,
Kung-Chun Lu ^c, Chin-Hsiung Loh ^c

^a Dept. of Civil and Environmental Engineering, Stanford Univ., Stanford, CA 94305, USA

^b Dept. of Civil and Environmental Engineering, Univ. of Michigan, Ann Arbor, MI 48109, USA

^c Dept. of Civil Engineering, National Taiwan Univ., Taipei, Taiwan

* Correspondence Author:

Prof. Kincho H. Law

Department of Civil and Environmental Engineering

Stanford University

Stanford, CA 94305-4020, USA

Tel. (650) 725-3154

Fax. (650) 723-7514

E-mail: law@stanford.edu

ABSTRACT

This paper discusses the potential use of wireless communication and embedded computing technologies for structural control applications. Specifically, control strategies based on linear quadratic regulator (LQR) algorithms are explored to assess the issues and performance for a prototype wireless structural sensing and control system. The system computes control decisions based on decentralized output feedback. The performance of this prototype system is first validated in shake table experiments using a half-scale three-story steel structure instrumented with three magnetorheological dampers, which are commanded by the prototype wireless sensing and control units. The experiments validate the effectiveness of the decentralized output feedback control algorithm. Further numerical simulations are conducted using the structural models of a 5-story and a 20-story structure controlled by ideal actuators and semi-active hydraulic dampers. The simulation analyses are intended to study the effects of communication latencies and degrees of centralization on control performance. Experimental and numerical results demonstrate that decentralized wireless control is viable for future structural control systems.

Keywords: structural control, wireless communication, embedded computing, decentralized control, output feedback control.

INTRODUCTION

For the past three decades, significant research and development have been conducted in the field of structural control to mitigate excessive responses (Soong and Spencer 2002, Chu *et al.*, 2005). Structural control systems can be categorized into three major types: (a) passive control (e.g. base isolation), (b) active control (e.g. active mass dampers), and (c) semi-active control (e.g. semi-active variable dampers). Passive control systems, e.g. base isolators, entail the use of passive energy dissipation devices to control the response of a structure without the use of sensors and controllers. Active control systems use a small number of large dampers or actuators for direct application of control forces. In a semi-active control system, control devices are used for indirect application of control forces. Semi-active control is currently preferred over active control because it can achieve at least an equivalent level of performance, consumes orders of magnitude less power, and provides higher level of reliability. Examples of semi-active actuators include active variable stiffness (AVS) devices, semi-active hydraulic dampers (SHD), electrorheological (ER) dampers, and magnetorheological (MR) dampers. Additional advantages associated with semi-active control include adaptability to real-time excitation, inherent Bounded Input/Bounded Output (BIBO) stability, and invulnerability against power failure. The shift from active control to semi-active control devices, which are smaller, less costly and more energy-efficient, will lead to the potential deployment of larger quantities of devices in a structure.

In a semi-active control system, sensors are deployed in the structure to collect structural response data during dynamic excitation. Response data is then fed into controllers to determine required actuation forces and to apply control commands to system actuators. Commanded by control signals, the actuators can generate control forces intended to mitigate undesirable structural responses. In traditional semi-active control systems, coaxial wires are normally used to provide communication links between sensors, actuators and controllers. With the rapid emergence of wireless

communication and embedding computing technologies, there have been extensive studies towards the development of wireless sensing technologies for structural monitoring applications (Straser and Kiremidjian 1998, Lynch and Loh 2006, Wang *et al.* 2007a). The adoption of wireless sensing technologies can remedy the high installation cost of commercial cable-based data acquisition (DAQ) systems, which can cost up to a few thousand dollars per sensing channel (Celebi 2002). A natural extension of the wireless sensing technology, as it matures, is to explore its applicability for semi-active or active control devices by eradicating cables associated with traditional control systems, which may result in substantial cost in installation time and expense (Solomon *et al.* 2000).

Extending the functionalities of a wireless sensor by including an actuation interface, the authors have developed a prototype wireless sensing and control system and explored the application to real-time feedback control in a laboratory setting (Wang *et al.* 2006, Wang *et al.* 2007b). When replacing wired communication channels with wireless ones for feedback structural control, issues such as coordination of sensing and control units, communication range, time delay and potential data loss need to be examined. Time delay due to wireless communication will cause degradation of the real-time performance of a control system (Lynch and Tilbury 2005). The time delay problem is common for any distributed network control systems, regardless of using wired or wireless communication (Lian *et al.* 2002). Decentralized control strategies may potentially resolve some of the difficult issues (Sandell *et al.* 1978, Siljak 1991, Lynch and Law 2002). In decentralized control, the control problem is divided into a collective set of smaller, distributed control sub-systems. Controllers assigned to a subsystem require only local and neighboring sensor data to make control decisions. In a wireless network, this leads to reduced use of the communication channel and results in higher control sampling rates. Shorter communication ranges may also enable more reliable data transmissions. Control computations can be performed in parallel using wireless sensors in decentralized control architectures. However, decentralized control may only achieve sub-optimal control performance when comparing to centralized control, because each subsystem only has local and neighboring sensor information to make control decisions. The purpose of this work is to examine the effectiveness of decentralized wireless sensing and control.

In this study, a linear quadratic regulator (LQR) feedback control algorithm is employed for both experimental and numerical simulations. A decentralized LQR control algorithm taking into consideration of time delays is first introduced. Experimental results from large-scale shake table structural control experiments conducted on a 3-story steel frame structure installed with MR dampers using a prototype wireless sensing and control system are then briefly reviewed (Wang *et al.* 2007b). The purpose of the experiments is to assess the viability of a wireless sensing and control system, and the performance of different decentralized and centralized control schemes. To further examine the issues involved in decentralized control and communication time delays, numerical simulations are conducted using a 5-story and a 20-story structural model controlled by ideal actuators and semi-active hydraulic dampers (SHD) (Kurata *et al.* 1999).

LQR CONTROL ALGORITHMS WITH TIME-DELAY USING OUTPUT FEEDBACK

A linear quadratic regulator (LQR) output feedback control algorithm that takes into consideration of time delay is summarized below. Consider a lumped-mass structural model with n degrees-of-freedom (DOF) and m actuators. The system state-space equations considering l time steps of delay can be stated as:

$$\mathbf{z}_d[k+1] = \mathbf{A}_d \mathbf{z}_d[k] + \mathbf{B}_d \mathbf{p}_d[k-l], \text{ where } \mathbf{z}_d[k] = \begin{Bmatrix} \mathbf{x}_d[k] \\ \dot{\mathbf{x}}_d[k] \end{Bmatrix} \quad (1)$$

In Eq. (1), $\mathbf{z}_d[k]$ and $\mathbf{p}_d[k-l]$ represent, respectively, the $2n \times 1$ discrete-time state-space vector at time k and the $m \times 1$ control force vector with time delay. The matrices \mathbf{A}_d and \mathbf{B}_d are the $2n \times 2n$ system matrix and the $2n \times m$ actuator location matrix, respectively. The objective to minimize a cost function J :

$$J|_{\mathbf{p}_d} = \sum_{k=l}^{\infty} (\mathbf{z}_d^T[k] \mathbf{Q} \mathbf{z}_d[k] + \mathbf{p}_d^T[k-l] \mathbf{R} \mathbf{p}_d[k-l]), \text{ where } \mathbf{Q}_{2n \times 2n} \geq 0 \text{ and } \mathbf{R}_{m \times m} > 0 \quad (2)$$

by selecting an optimal control force trajectory \mathbf{p}_d . Let the system output be denoted by a $q \times 1$ system vector $\mathbf{y}_d[k]$ measured at time k . The state-space vector $\mathbf{z}_d[k]$ and output vector $\mathbf{y}_d[k]$ can be related by a $q \times 2n$ linear transformation, \mathbf{D}_d , that is:

$$\mathbf{y}_d[k] = \mathbf{D}_d \mathbf{z}_d[k] \quad (3)$$

The optimal output feedback control force \mathbf{p}_d can be computed using an $m \times q$ gain matrix \mathbf{G}_d as:

$$\mathbf{p}_d[k] = \mathbf{G}_d \mathbf{y}_d[k] \quad (4)$$

where the gain matrix \mathbf{G}_d is designed so that the cost function J is minimized.

For the output feedback control problem with time delay (say, l time steps), Chung *et al.* (1995) propose a solution by introducing a modified first-order difference equation:

$$\bar{\mathbf{z}}_d[k+1] = \bar{\mathbf{A}}_d \bar{\mathbf{z}}_d[k] + \bar{\mathbf{B}}_d \bar{\mathbf{p}}_d[k] \quad (5)$$

This modified first-order difference system is equivalent to the original system (Eq. 1) by proper definitions of the augmented matrices and vectors:

$$\bar{\mathbf{A}}_d = \begin{bmatrix} \mathbf{A}_d & \mathbf{0} & \cdots & \mathbf{0} & \mathbf{0} \\ \mathbf{I} & \mathbf{0} & \cdots & \mathbf{0} & \mathbf{0} \\ \mathbf{0} & \mathbf{I} & \cdots & \mathbf{0} & \mathbf{0} \\ \vdots & \vdots & \ddots & \vdots & \vdots \\ \mathbf{0} & \mathbf{0} & \cdots & \mathbf{I} & \mathbf{0} \end{bmatrix}, \quad \bar{\mathbf{B}}_d = \begin{bmatrix} \mathbf{B}_d \\ \mathbf{0} \\ \mathbf{0} \\ \vdots \\ \mathbf{0} \end{bmatrix}, \quad \bar{\mathbf{z}}_d[k] = \begin{bmatrix} \mathbf{z}_d[k] \\ \mathbf{z}_d[k-1] \\ \vdots \\ \mathbf{z}_d[k-l] \end{bmatrix}, \quad \bar{\mathbf{p}}_d[k] = \mathbf{p}_d[k-l] \quad (6)$$

where $\mathbf{0}$ and \mathbf{I} represent, respectively, the zero and identity submatrices of proper dimensions. Correspondingly, the weighting matrix in Eq. (2) and the output matrix in Eq. (3) are also augmented and denoted by $\bar{\mathbf{Q}}$ and $\bar{\mathbf{D}}_d$, respectively, as:

$$\bar{\mathbf{Q}} = \begin{bmatrix} \mathbf{Q} & \mathbf{0} & \cdots & \mathbf{0} & \mathbf{0} \\ \mathbf{0} & \mathbf{0} & \cdots & \mathbf{0} & \mathbf{0} \\ \mathbf{0} & \mathbf{0} & \cdots & \mathbf{0} & \mathbf{0} \\ \vdots & \vdots & \ddots & \vdots & \vdots \\ \mathbf{0} & \mathbf{0} & \cdots & \mathbf{0} & \mathbf{0} \end{bmatrix}, \quad \bar{\mathbf{D}}_d = [\mathbf{0} \quad \mathbf{0} \quad \cdots \quad \mathbf{0} \quad \mathbf{D}_d] \quad (7)$$

In order to make the optimization problem independent of the initial state, $\bar{\mathbf{z}}_d[l]$, which contains the state space vectors $\mathbf{z}_d[0], \dots, \mathbf{z}_d[l]$, is considered as a random vector. The design objective is altered to minimize the expected value of the original cost J :

$$\bar{J} = E\{J\} \quad (8)$$

where $E\{\cdot\}$ denotes the expectation. Let $\bar{\mathbf{Z}}_{dl}$ represent the second statistical moment of the augmented initial state:

$$\bar{\mathbf{Z}}_{dl} = E\{\bar{\mathbf{z}}_d[l] \bar{\mathbf{z}}_d^T[l]\} \quad (9)$$

It can be shown that by introducing an auxiliary matrix \mathbf{H} , the expected cost is equivalent to (Chung et al 1995):

$$\bar{J} = E\{\bar{\mathbf{z}}_d^T[l] \mathbf{H} \bar{\mathbf{z}}_d[l]\} = \text{trace}\{\mathbf{H} \bar{\mathbf{Z}}_{dl}[l]\} \quad (10)$$

In practice, it is generally assumed that initial state $\bar{\mathbf{z}}_d[l]$ is a random variable uniformly distributed on the surface of the unit sphere, i.e. $\bar{\mathbf{Z}}_d = \mathbf{I}$. Finally, the control problem with time delay can be posed as solving the following nonlinearly coupled matrix equations:

$$(\bar{\mathbf{A}}_d + \bar{\mathbf{B}}_d \mathbf{G}_d \bar{\mathbf{D}}_d)^T \mathbf{H} (\bar{\mathbf{A}}_d + \bar{\mathbf{B}}_d \mathbf{G}_d \bar{\mathbf{D}}_d) - \mathbf{H} + (\bar{\mathbf{Q}} + \bar{\mathbf{D}}_d^T \mathbf{G}_d^T \mathbf{R} \mathbf{G}_d \bar{\mathbf{D}}_d) = \mathbf{0} \quad (11a)$$

$$(\bar{\mathbf{A}}_d + \bar{\mathbf{B}}_d \mathbf{G}_d \bar{\mathbf{D}}_d) \mathbf{L} (\bar{\mathbf{A}}_d + \bar{\mathbf{B}}_d \mathbf{G}_d \bar{\mathbf{D}}_d)^T - \mathbf{L} + \bar{\mathbf{Z}}_d = \mathbf{0} \quad (11b)$$

$$2\bar{\mathbf{B}}_d^T \mathbf{H} (\bar{\mathbf{A}}_d + \bar{\mathbf{B}}_d \mathbf{G}_d \bar{\mathbf{D}}_d) \mathbf{L} \bar{\mathbf{D}}_d^T + 2\mathbf{R} \mathbf{G}_d \bar{\mathbf{D}}_d \mathbf{L} \bar{\mathbf{D}}_d^T = \mathbf{0} \quad (11c)$$

where \mathbf{G}_d is the optimal output feedback gain matrix, \mathbf{L} is the Lagrangian matrix and \mathbf{H} is an auxiliary matrix. Details on the derivation of the time-delay optimal control solution have been described by Chung *et al.* (1995).

In this study, an iterative algorithm described by Lunze (1990) is employed for the time delay problem. Furthermore, the algorithm is modified for decentralized control by constraining the structure of the gain matrix \mathbf{G}_d to be consistent with the decentralized architecture. As shown in Fig. 1, the iterative algorithm starts from an initial estimate for the gain matrix \mathbf{G}_d . Within each iteration step i , the matrix \mathbf{H}_i and \mathbf{L}_i are solved respectively using the current estimate of the gain matrix \mathbf{G}_{di} . Based on the \mathbf{H}_i and \mathbf{L}_i matrices computed, a search gradient Δ_i is calculated and the new gain matrix \mathbf{G}_{di+1} is computed by traversing along the gradient from \mathbf{G}_{di} . An adaptive multiplier, s , is used to dynamically control the search step size. At each iteration step, two conditions are used to decide whether \mathbf{G}_{di+1} is an acceptable estimate. The first condition is $\text{trace}(\mathbf{H}_{i+1} \bar{\mathbf{Z}}_d) < \text{trace}(\mathbf{H}_i \bar{\mathbf{Z}}_d)$ which guarantees that \mathbf{G}_{di+1} is a better solution than \mathbf{G}_{di} . The second condition is that the maximum magnitude of all the eigenvalues of the matrix $(\bar{\mathbf{A}}_d + \bar{\mathbf{B}}_d \mathbf{G}_{di+1} \bar{\mathbf{D}}_d)$ needs to be less than 1 to ensure the stability of the augmented system. To find the gain matrix \mathbf{G}_d that is consistent with the decentralized architectural constraints, the gradient matrix Δ_i computed using Eq. 11c is modified by zeroing out those entries

which correspond to the zero terms in the decentralized output feedback gain matrix. The iteration then proceeds to compute the next estimate $\mathbf{G}_{d_{i+1}}$ by traversing along this constrained gradient.

A PROTOTYPE WIRELESS STRUCTURAL SENSING AND CONTROL SYSTEM

The prototype wireless sensing and control system is built upon the previous developed wireless sensing unit designed for structural sensing and monitoring applications (Wang *et al.* 2005, 2007a). The wireless sensing unit consists of three basic functional modules: the sensor signal digitizer, the computational core, and the wireless transceiver (see Fig. 2a). A simple two-layer printed circuit board (PCB) is designed for the wireless sensing unit, which, including the batteries, fits within an 10.2cm by 6.5cm by 4.0cm off the shelf weatherproof plastic container (see Fig. 2b). To extend the functionality of the wireless sensor for actuation, an off-board control signal generation module (Fig. 2c) is designed and fabricated. A separate 5.5cm by 6.0cm PCB is designed for the control signal generation module which consists of a single-channel 16-bit digital-to-analog converter (Analog Device AD5542) and other support electronics. As shown in Fig. 2d, the control signal module is attached to the wireless sensing unit via two multi-line wires – one for analog signals and the other one for digital signals. The module can output an analog voltage from -5V to 5V at rates as high as 100 kHz. Detailed design of the wireless sensing and control unit and the control signal generation module has been described by Wang *et al.* (2006, 2007b).

To study the potential application of the wireless sensing and control system for structural control, validation tests on a 3-story frame structure instrumented with MR dampers are conducted at the National Center for Research on Earthquake Engineering (NCREE) in Taipei, Taiwan (see Fig. 3). This section first introduces the experimental setup, and then presents the test results. The three-story steel frame structure has a 3m by 2m floor plan, 3m inter-story height, and a weight adjusted to 6,000 kg per each floor using concrete blocks. Both the beams and the columns of the structure are

constructed with H150 × 150 × 7 × 10 steel I-beam elements. The three-story structure is mounted on a 5m × 5m 6-DOF shake table. For this study, only longitudinal excitations are used. Along this direction, the shake table can excite the structure with a maximum acceleration of 9.8m/s². The test structure is heavily instrumented with accelerometers, velocity meters, and linear variable displacement transducers (LVDT) installed on each floor of the structure to measure the dynamic response. These sensors are interfaced to a high-precision wire-based data acquisition (DAQ) system resided at the NCREE facility; the wire-based DAQ system is set to a sampling rate of 200 Hz.

The basic architecture of the prototype wireless sensing and control system is schematically shown in Fig. 3a. Wireless sensors and controllers are mounted on the structure for measuring structural response data and commanding the actuators in real-time. In addition to the wireless sensing and control units, a remote data and command server with a wireless transceiver is included as an optional element responsible for logging the flow of wireless data. During an experimental test, the command server first notifies the wireless sensing and control units to initiate automated operations. Once the start command is received, the wireless units that are responsible for collecting sensor data start acquiring and broadcasting data at a specified time interval. Accordingly, the wireless units responsible for commanding the actuators receive the sensor data, calculate desired control forces in real-time, and apply control commands at the specified time interval.

For this experimental study, three 20 kN MR dampers are installed with V-braces on each story of the steel structure (Fig. 3c). The damping coefficients of the MR dampers can be changed by issuing a command voltage between 0V to 1.2V. This command voltage determines the electric current of the electromagnetic coil in the MR damper, which in turn, generates a magnetic field that sets the viscous damping properties of the MR damper. Calibration tests are first conducted on the MR dampers before mounting them to the structure so that modified Bouc-Wen damper models can be formulated for each damper (Lin *et al.* 2005). In the real-time feedback control tests, hysteresis model parameters for the MR dampers are an integral element in the calculation of damper actuation voltages. For

wireless sensing and control, a separate wire is used to output the appropriate voltage from the off-board control generation module to command the MR dampers (see Fig. 3d).

For the wireless system, a total of four wireless sensors are installed, following the schematic shown in Fig. 3(a). Each wireless sensor is interfaced to a Tokyo Sokushin VSE15-D velocity meter to measure the absolute velocity response for each floor of the structure as well as the base. The sensitivity of this velocity meter is 10V/(m/s) with a measurement limit of ± 1 m/s. The three wireless sensors on the first three levels of the structure (C_0 , C_1 , and C_2) are also responsible for commanding the MR dampers. Besides the wireless control system, a traditional wire-based control system is installed in the structure for comparative tests.

Centralized and decentralized velocity feedback control schemes are used for the wired and the wireless control systems. For the centralized control tests, the output vector includes the relative velocities (but not the relative displacements) on all floors with respect to the ground; the output matrix, \mathbf{D}_d , thus has the form:

$$\mathbf{D}_{d1} = [\mathbf{0}_{3 \times 3} \quad \mathbf{I}_{3 \times 3}] \quad (12)$$

For decentralized control tests, the inter-story velocities between adjacent floors are defined as the output vector, and the output matrix \mathbf{D}_d is set to have the form:

$$\mathbf{D}_{d2} = \left[[\mathbf{0}_{3 \times 3}] \begin{bmatrix} 1 & 0 & 0 \\ -1 & 1 & 0 \\ 0 & -1 & 1 \end{bmatrix} \right] \quad (13)$$

Furthermore, to represent a fully decentralized, partially decentralized and centralized control schemes, the output feedback gain matrices for the 3-story test structure are constrained to the following respective patterns:

$$\mathbf{G}_{d1} = \begin{bmatrix} * & 0 & 0 \\ 0 & * & 0 \\ 0 & 0 & * \end{bmatrix}, \quad \mathbf{G}_{d2} = \begin{bmatrix} * & * & 0 \\ 0 & * & * \\ 0 & * & * \end{bmatrix} \text{ and } \mathbf{G}_{d3} = \begin{bmatrix} * & * & * \\ * & * & * \\ * & * & * \end{bmatrix} \quad (14)$$

When combined with the output matrix \mathbf{D}_d defined in Eq. (12) or (13), the pattern in \mathbf{G}_{d1} specifies that when computing control decisions, the actuator at each floor only needs the entry in the output vector \mathbf{y}_d corresponding to that floor. The pattern in \mathbf{G}_{d2} specifies that the control decisions require information from a neighboring floor. Finally, the pattern in \mathbf{G}_{d3} indicates all entries in the output vector participate in the centralized control decisions.

Table 1 summarizes the different patterns of the gain matrix \mathbf{G}_d , the output matrices \mathbf{D}_d , and the achievable sampling times for the centralized, partially decentralized and fully decentralized control strategies (which are denoted by degrees of decentralization, 3, 2 and 1, respectively). For this test structure, the wire-based system can achieve a sampling rate of 200Hz, or a time step of 0.005s. Mostly decided by the communication latency of the 24XStream wireless transceivers, the wireless system can achieve a sampling rate of 12.5Hz (or a time step of 0.08s) for the centralized control scheme. This sampling rate is due to each wireless sensor waiting in turn to communicate its data to the network (about 0.02s for each transmission). An advantage of the decentralized architecture is that fewer communication steps are needed, thereby reducing the time for wireless communication.

To ensure that appropriate control decisions are computed by the wireless control units, one necessary condition is that the real-time velocity data used by the control units are reliable. Rarely experiencing data losses during the experiments, our prototype wireless sensor network proves to be robust. In case data loss happens, the wireless control unit is currently designed to simply use a previous data sample. For the experimental results presented herein, the ground excitation is the 1940 El Centro NS earthquake record (Imperial Valley Irrigation District Station) scaled to a peak ground acceleration of 1m/s^2 . To illustrate the performance of different decentralized schemes with different communication

latencies, the same ground excitation is applied to the original uncontrolled structure and the structure controlled by the four different wireless and wired control schemes as defined in Table 1. Fig. 4 illustrates the structure's peak inter-story drifts and floor accelerations during these experimental runs. Compared with the uncontrolled structure, all wireless and wired control schemes achieve significant reduction with respect to maximum inter-story drifts and absolute accelerations. Among the four control cases, the wired centralized control scheme shows better performance in achieving the least peak drifts and second least overall peak accelerations. This result is rather expected, because the wired system has the advantages of lower communication latency and utilizes complete sensor data from all floors. The wireless schemes, although running at longer sampling steps, achieve control performance comparable to the wired system. The fully decentralized wireless control scheme (case #1), results in uniform peak inter-story drifts and the least peak floor accelerations. This illustrates that in the decentralized wireless control cases, the higher sampling rate (from lower communication latency) can potentially compensate the loss of data from ignoring the sensor data from faraway floors.

NUMERICAL SIMULATIONS ON DECENTRALIZED STRUCTURAL CONTROL

With encouraging results from the experimental tests, further investigations of the decentralized output feedback control strategies are performed with numerical simulations. Specifically, different decentralization patterns and sampling time delays are being investigated for two structural models, namely a 5-story Kajima-Shizuoka building (Kurata et al 1999) and a 20-story benchmark structure designed for the Structural Engineers Association of California (SAC) project (Spencer et al 1998). Numerical simulation results are performed for the cases when the structures are instrumented with ideal actuators that are capable of producing any desired forces and with semi-active hydraulic dampers (SHD). The actuators are installed as a V-brace on each floor of the structures (see Fig. 5). For the SHD dampers, the Maxwell element proposed by Hatada *et al.* (2000) is employed to model the damping force and is described by the following differential equation:

$$\dot{p}(t) + \frac{k_{eff}}{c_{SHD}(t)} p(t) = k_{eff} \Delta \dot{x}(t) \quad (15)$$

where $p(t)$ and $\Delta \dot{x}(t)$ denote the damping force and the inter-story velocity, respectively, k_{eff} represents the effective stiffness of the damper in series with the V-brace, and $c_{SHD}(t)$ is the adjustable damping coefficient of the SHD damper. If the desired damper force is in an opposite direction to the inter-story velocity, as shown in Fig. 5, the damping coefficient is adjusted so that a damper force closest to the desired force is generated. If the desired force is in the same direction to the inter-story velocity, the damping coefficient is set to its minimum value.

DECENTRALIZED STRUCTURAL CONTROL SIMULATIONS OF A 5-STORY BUILDING

A five-story model similar to the Kajima-Shizuoka Building is employed (Kurata *et al.*, 1999). The steel-structure building has a total height of about 19m (Fig. 6). For this study, two semi-active hydraulic dampers (SHD) are installed at each floor.

In the numerical simulations, it is assumed that both the inter-story displacement and inter-story velocity relative to the lower floor are measurable. Similarly, the state-space system is formulated such that the state-space vector contains inter-story displacements and inter-story velocities, rather than the displacements and velocities relative to the ground. In order to reflect this requirement on sensor data, the output matrix \mathbf{D}_d is defined to be a $2n \times 2n$ identity matrix. The simulations are conducted for different degrees of centralization (DC), as illustrated in Fig. 6(b); the case where DC equal to i represents that the neighboring i floors constitute a communication subnet and share their sensor data. For example, the case where DC=1 implies each group consists of only one floor. For the case where DC=3, each group consists of three floors, resulting in 3 wireless subnets for the 5 story building. For DC=5, all 5 floors share their sensor data, resulting in a centralized information architecture. Based on the above definitions for output matrix \mathbf{D}_d and degrees of centralization, the

gain matrix consists of two square submatrices with the same symmetric shape constraints. In each square submatrix, the diagonal entries and the j^{th} ($j = 1, \dots, i-1$) entry above and below the diagonal entry are non-zero. For example, when DC = 2, the gain matrix has the following shape constraint:

$$\mathbf{G}_d = \left[\begin{array}{cc|cc} * & * & 0 & 0 & 0 & * & * & 0 & 0 & 0 \\ * & * & * & 0 & 0 & * & * & * & 0 & 0 \\ 0 & * & * & * & 0 & 0 & * & * & * & 0 \\ 0 & 0 & * & * & * & 0 & 0 & * & * & * \\ 0 & 0 & 0 & * & * & 0 & 0 & 0 & * & * \end{array} \right]_{5 \times 10} \quad (16)$$

The left submatrix and the right submatrix correspond to the displacement part and the velocity part, respectively, of the output vector \mathbf{y}_d . The various combinations of centralization degrees (1 through 5) and sampling time steps ranging from 0.005s to 0.06s (at a resolution of 0.005s) are simulated. Four ground motion records are used for each simulation: the 1940 El Centro NS record (Imperial Valley Irrigation District Station) scaled to a peak ground acceleration (PGA) of 1m/s², the same 1940 El Centro NS record scaled to a PGA of 2m/s², the 1999 Chi-Chi NS record (TCU-076 Station) scaled to a PGA of 1m/s², and the 1995 Kobe NS record (JMA Station) scaled to a PGA of 1m/s². Performance indices proposed by Spencer *et al.* (1998) are adopted. In particular, the two representative performance indices employed are:

$$PI_1 = \max_{\text{Earthquakes}} \left\{ \frac{\max_{t,i} d_i(t)}{\max_{t,i} \hat{d}_i(t)} \right\}, \text{ and } PI_2 = \max_{\text{Earthquakes}} \left\{ \frac{J_{LQR}}{\hat{J}_{LQR}} \right\} \quad (17)$$

Here PI_1 and PI_2 are the performance indices corresponding to inter-story drifts and LQR cost indices, respectively. In Eq. (17), $d_i(t)$ represents the inter-story drift between floor i ($i = 1, \dots, 5$) and its lower floor at time t , and $\max_{t,i} d_i(t)$ is the maximum inter-story drift over the entire time history and among all floors. The maximum inter-story drift is normalized by its counterpart $\max_{t,i} \hat{d}_i(t)$, which is the maximum response of the uncontrolled structure. The largest normalized ratio among the

simulations for the four different earthquake records is defined as the performance index PI_1 .

Similarly, the performance index PI_2 is defined for the LQR control index J_{LQR} , as given in Eq. (2).

When computing the LQR index over time, a uniform time step of 0.001s is used to collect the structural response data points, regardless of the sampling time step of the control scheme; this allows one control strategy to be compared to another without concern for the different sampling time steps used in the control solution.

Fig. 7 and Fig. 8 show the values of the two control performance indices for the 5-story structure instrumented with ideal actuators and SHD dampers, respectively. Different combinations of degrees of centralization and sampling time steps are employed for the simulations. The plots clearly illustrate that the degrees of centralization and sampling steps could have significant impact on the performance of the control system. Generally speaking, control performance is better for higher degrees of centralization and shorter sampling times. To better review the simulation results, the performance indices for the five different control schemes are also plotted as a function of sampling time. For example, as shown in Fig. 8(c), if a partially decentralized control system with DC equal to 2 can achieve 0.01s sampling step and a centralized system can only achieve 0.03s due to additional communication latency, the partially decentralized system can result in much lower maximum inter-story drifts. Similar trends are observed in Fig. 8(d) for the LQR performance indices.

DECENTRALIZED STRUCTURAL CONTROL SIMULATIONS OF A 20-STORY BUILDING

A 20-story benchmark structure designed for the Structural Engineers Association of California (SAC) project is also selected for numerical simulations (Spencer *et al.*, 1998). To simplify the analysis, the building is modeled as an in-plane lumped-mass structure (Fig. 9). In the numerical simulations, it is assumed that both the inter-story displacements and inter-story velocities between every two

neighboring floors are measurable. The system state-space equations are formulated such that the state-space vector contains inter-story displacements and velocities, rather than the displacements and velocities relative to the ground. The output matrix \mathbf{D}_d is defined as a $2n \times 2n$ identity matrix, as in the case of the 5-story structure, so that the state-space vector is used for control feedback directly. The simulations are conducted for different degrees of centralization (DC), as illustrated in Fig. 9(c). The degrees of centralization reflect different communication network architectures, with each channel representing one communication subnet. The actuators covered within a subnet are allowed to access the wireless sensor data within that subnet. For example, the case where DC=1 implies each wireless channel covers only five stories and a total of four wireless channels (subnets) are utilized. Of all the different degrees of centralization, the case where DC=1 represents the lowest requirement to the wireless communication range and achieves lowest communication latency as a smaller number of wireless sensors need to broadcast their data in the subnet. Constrained by this decentralized information structure, the gain matrix for the case where DC=1 has the following sparsity pattern:

$$\mathbf{G}_d = \left[\begin{array}{c|c} \mathbf{G}^{(1,1)} & \mathbf{G}^{(1,5)} \\ \mathbf{G}^{(2,2)} & \mathbf{G}^{(2,6)} \\ \mathbf{G}^{(3,3)} & \mathbf{G}^{(3,7)} \\ \hline & \mathbf{G}^{(4,8)} \end{array} \right]_{20 \times 40}, \text{ when DC = 1} \quad (18)$$

The left submatrix and the right submatrix correspond to the inter-story displacement and the inter-story velocity components, respectively, of the output vector \mathbf{y}_d . The left and right submatrices are block-diagonal, with every block $\mathbf{G}^{(i,j)}$ being a 5-by-5 square matrix. For the case where DC=2, each wireless channel covers ten stories and a total of three wireless channels are utilized. Constrained by the overlapping information structure, the gain matrix for DC=2 has the following sparsity pattern:

$$\mathbf{G}_d = \begin{bmatrix} \mathbf{G}^{(1,1)} & \mathbf{G}^{(1,2)} \\ \mathbf{G}^{(2,1)} & \mathbf{G}^{(2,2)} & \mathbf{G}^{(2,3)} \\ & \mathbf{G}^{(3,2)} & \mathbf{G}^{(3,3)} & \mathbf{G}^{(3,4)} \\ & \mathbf{G}^{(4,3)} & \mathbf{G}^{(4,4)} \end{bmatrix} \begin{bmatrix} \mathbf{G}^{(1,5)} & \mathbf{G}^{(1,6)} \\ \mathbf{G}^{(2,5)} & \mathbf{G}^{(2,6)} & \mathbf{G}^{(2,7)} \\ & \mathbf{G}^{(3,6)} & \mathbf{G}^{(3,7)} & \mathbf{G}^{(3,8)} \\ & \mathbf{G}^{(4,7)} & \mathbf{G}^{(4,8)} \end{bmatrix}_{20 \times 40}, \text{ when DC} = 2 \quad (19)$$

For the case when DC=3, the number of stories covered by each of the two wireless subnets increases accordingly. That leads to fewer communication subnets and fewer zero blocks in the gain matrices. The case where DC=4 specifies that one wireless channel covers all twenty floors, which results in a centralized information structure.

Fig. 10 shows the numerical simulation results for the 20-story structure instrumented with ideal actuators. Various combinations of centralization degrees (DC = 1,...,4) and sampling time steps ranging from 0.01s to 0.06s (at a resolution of 0.01s) are simulated. Three ground motion records are used for each simulation: the 1940 El Centro NS record (Imperial Valley Irrigation District Station), the 1995 Kobe NS record (JMA Station), and the 1999 Chi-Chi NS record (TCU-076 Station), all scaled to a peak ground acceleration (PGA) of 1m/s². The two performance indices introduced in Eq. (17) are plotted in Fig. 10 for different combinations of degrees of centralization and sampling time steps. Similar to the simulations for the 5-story structural model, when computing the LQR index over time, a uniform time step of 0.001s is used to collect the structural response data points, regardless of the sampling time step of the control scheme. Generally speaking, the results are similar to the previous results for the 5-story structure where the control performance is better for higher degrees of centralization and shorter sampling times. The plots show that except for the case where DC=1, the control schemes with certain overlapping information structures achieve comparable performance. As shown in Fig. 10(c), if a partially decentralized control system with DC equal to 2 can achieve a sampling step of 0.02s and a centralized system can only achieve 0.04s due to additional communication latency, the partially decentralized system can result in lower maximum inter-story drifts. Similar trends are observed in Fig. 10(d), except that the plots are smoother due to the summation process for computing the LQR indices.

Numerical simulations are also conducted for the four control strategies where semi-active hydraulic dampers (SHD) are employed on the structure. The arrangement of SHD dampers is shown in Fig. 9(d); the number of instrumented SHD dampers decreases gradually from 4 to 1 in the higher floors. Fig. 11 presents the simulated maximum inter-story drifts when the structure is excited using the same three ground motions, except that the PGAs are scaled up to 5m/s^2 , instead of 1m/s^2 . To compare the performance of decentralized versus centralized control, the case where DC=2 (partially decentralized) and the case where DC=4 (centralized) are plotted. As shown in Fig. 9, each subnet covers ten floors when DC=2, or twenty floors when DC=4. That is, the induced time delay when DC=2 is about half of the delay when DC=4, and the time delays of 20ms and 40ms are assigned, respectively, for these two cases. As shown in Fig. 11, both of the two control schemes significantly reduce the maximum inter-story drifts compared with the uncontrolled case. For the Kobe and Chi-Chi ground motions, the partially decentralized case where DC=2 achieves equivalent performance compared with the centralized case where DC=4, while for the El Centro record, the case with DC=2 achieves slightly better performance than the case where DC=4. These results illustrate that although decentralized control has the disadvantage of computing control decisions without complete sensor data, the lower time delay in decentralized control could make the control scheme perform as well as centralized control, given that the centralized case, using wireless communication, requires longer latencies.

CONCLUSIONS

In this paper, a prototype wireless structural sensing and control system is presented. The performance of the prototype system has been successfully validated in real-time feedback control experiments using a 3-story steel structure instrumented with MR dampers. The experiments have also shown the potential effectiveness of decentralized output feedback control. Using the LQR-based decentralized control algorithm, simulation results are obtained for a 5-story and a 20-story building structure instrumented with ideal actuators and SHD dampers, by varying the degrees of centralization and the

sampling time steps of the control system. Both the experimental results and the simulations results demonstrate that decentralized wireless sensing and control is viable for future structural control systems. It is also illustrated that decentralized control strategies may provide equivalent or even superior control performance, given that their centralized counterparts could suffer longer feedback time delay due to wireless communication latencies.

Future research will continue to investigate both the theory and implementation of wireless decentralized structural control. Besides LQR, other decentralized control algorithms that may achieve better control performance are worth exploring. Initial progress has been made in developing decentralized \mathcal{H}_∞ control algorithms, where decentralized controllers are designed to minimize the \mathcal{H}_∞ norm of the closed-loop system transfer matrix (Zhou *et al.* 1996). For implementation, system performance can be greatly improved by employing more powerful embedded computing devices, and adopting wireless technologies that have lower communication latency (such as IEEE 802.11 and 802.15.4 standards). Further wireless structural sensing and control experiments using a larger-scale laboratory structure are being planned to gain better understanding of decentralized control strategies.

ACKNOWLEDGMENTS

This research is partially funded by the National Science Foundation under grants CMS-9988909 (Stanford University), CMS-0528867 (University of Michigan), and the Office of Naval Research Young Investigator Program awarded to Prof. Lynch at the University of Michigan. Additional support is provided by National Science Council in Taiwan under Grant No. NSC 94-2625-Z-002-031. The authors wish to thank the two fellowship programs: the Office of Technology Licensing Stanford Graduate Fellowship and the Rackham Grant and Fellowship Program at the University of Michigan. This paper is an extension of the article presented at the US-Taiwan Workshop on Smart Structures and Structural Health Monitoring in Taipei, Taiwan, October, 2006; the authors would like to acknowledge the travel supports provided by the National Science Foundation for attending the workshop.

REFERENCES

- Çelebi, M. (2002). *Seismic Instrumentation of Buildings (with Emphasis on Federal Buildings)*. Report No. 0-7460-68170, United States Geological Survey, Menlo Park, CA.
- Chu, S.Y., Soong, T.T. and Reinhorn, A.M. (2005), *Active, Hybrid, and Semi-active Structural Control: a Design and Implementation Handbook*, Wiley, Hoboken, NJ.
- Chung, L.L., Lin, C.C. and Lu, K.H. (1995). "Time-delay control of structures," *Earthq. Eng. Struct. D.*, **24**(5), 687-701.
- Hatada, T., Kobori, T., Ishida, M. and Niwa, N. (2000). "Dynamic analysis of structures with Maxwell model," *Earthq. Eng. Struct. D.*, **29**(2), 159-176.
- Kurata, N., Kobori, T., Takahashi, M., Niwa, N. and Midorikawa, H. (1999). "Actual seismic response controlled building with semi-active damper system," *Earthq. Eng. Struct. D.*, **28**(11), 1427-1447.
- Lian, F.-L., Moyne, J. and Tilbury, D. (2002). "Network design consideration for distributed control systems," *IEEE T. Contr. Syst. T.*, **10**(2), 297-307.
- Lin, P.-Y., Roschke, P.N. and Loh, C.-H. (2005). "System identification and real application of the smart magneto-rheological damper," *Proceedings of the 2005 International Symposium on Intelligent Control*, Limassol, Cyprus, June 27-29.
- Lunze, J. (1992), *Feedback Control of Large Scale Systems*, Prentice-Hall, New York.
- Lynch, J.P. and Law, K.H. (2002). "Decentralized control techniques for large scale civil structural systems," *Proceedings of the 20th International Modal Analysis Conference*, Los Angeles, CA, February 4-7.
- Lynch, J.P. and Tilbury, D.M. (2005). "Implementation of a decentralized control algorithm embedded within a wireless active sensor," *Proceedings of the 2nd Annual ANCRiSST Workshop*, Gyeongju, Korea, July 21-24.
- Lynch, J.P. and Loh, K.J. (2006). "A summary review of wireless sensors and sensor networks for structural health monitoring," *Shock Vib. Dig.*, **38**(2), 91-128.
- Sandell, N., Jr., Varaiya, P., Athans, M. and Safonov, M. (1978). "Survey of decentralized control methods for large scale systems," *IEEE T. Automat. Contr.*, **23**(2), 108-128.
- Siljak, D.D. (1991), *Decentralized control of complex systems*, Academic Press, Boston.
- Solomon, I., Cunnane, J. and Stevenson, P. (2000). "Large-scale structural monitoring systems," *Proceedings of SPIE Non-destructive Evaluation of Highways, Utilities, and Pipelines IV*, Newport Beach, CA, March 7-9.
- Soong, T.T. and Spencer, B.F., Jr. (2002). "Supplemental energy dissipation: state-of-the-art and state-of-the-practice," *Eng. Struct.*, **24**(3), 243-259.
- Spencer, B.F., Jr., Christenson, R.E. and Dyke, S.J. (1998). "Next generation benchmark control problem for seismically excited buildings," *Proceedings of the 2nd World Conference on Structural Control*, Kyoto, Japan, June 29 -July 2.
- Straser, E.G. and Kiremidjian, A.S. (1998). *A Modular, Wireless Damage Monitoring System for Structures*. Report No. 128, John A. Blume Earthquake Eng. Ctr., Stanford University, Stanford, CA.
- Wang, Y., Lynch, J.P. and Law, K.H. (2005). "Wireless structural sensors using reliable communication protocols for data acquisition and interrogation," *Proceedings of the 23rd International Modal Analysis Conference (IMAC XXIII)*, Orlando, FL, January 31 - February 3.
- Wang, Y., Swartz, R.A., Lynch, J.P., Law, K.H., Lu, K.-C. and Loh, C.-H. (2006). "Wireless feedback structural control with embedded computing," *Proceedings of the SPIE 11th International*

Symposium on Nondestructive Evaluation for Health Monitoring and Diagnostics, San Diego, CA, February 26 - March 2.

- Wang, Y., Lynch, J.P. and Law, K.H. (2007a). "A wireless structural health monitoring system with multithreaded sensing devices: design and validation," *Struct. and Infrastructure Eng.*, 3(2), 103-120.
- Wang, Y., Swartz, R.A., Lynch, J.P., Law, K.H., Lu, K.-C. and Loh, C.-H. (2007b). "Decentralized civil structural control using real-time wireless sensing and embedded computing," *Smart Struct. Syst.*, in press.
- Zhou, K., Doyle, J.C. and Glover, K. (1996), *Robust and optimal control*, Prentice Hall, Englewood Cliffs, N.J.

Keywords: structural control, wireless communication, embedded computing, decentralized control, output feedback control.

LIST OF FIGURES AND TABLES

Figure 1. Heuristic algorithm solving the coupled nonlinear matrix equations (Eq. 11) for decentralized optimal time-delay output feedback control (Lunze, 1990).

Figure 2. Overview to the prototype wireless sensing and actuation unit: (a) printed circuit board for the wireless sensing unit ($9.7 \times 5.8 \text{ cm}^2$); (b) packaged wireless sensing and control unit ($10.2 \times 6.5 \times 4.0 \text{ cm}^3$); (c) printed circuit board of the signal generation module ($5.5 \times 6.0 \text{ cm}^2$); (d) control signal module connected to wireless sensor.

Figure 3. Laboratory setup: (a) deployment scheme of wireless sensors and actuators; (b) the 3-story test structure mounted on the shake table; (c) the MR damper installed between the 1st floor and the base floor of the structure; (d) a wireless control unit and an off-board control signal generation module.

Figure 4. Experimental results of different control schemes using the El Centro excitation scaled to a peak acceleration of 1m/s^2 : (a) peak inter-story drifts; (b) peak accelerations.

Figure 5. Key parameters of the SHD damper employed.

Figure 6. A five-story model similar to the Kajima-Shizuoka Building: (a) side elevation of the building; (b) information group partitioning for different degrees of centralization (DC).

Figure 7. Simulation results for the five-story Kajima-Shizuoka Building instrumented with ideal actuators. The plots illustrate performance indexes for different sampling time steps and degrees of centralization (DC): (a) 3D plot for performance index PI_1 ; (b) 3D plot for performance index PI_2 ; (c) condensed 2D plot for PI_1 ; (d) condensed 2D plot for PI_2 .

Figure 8. Simulation results for the five-story Kajima-Shizuoka Building instrumented with semi-active hydraulic dampers (SHD). The plots illustrate performance indexes for different sampling time steps and degrees of centralization (DC): (a) 3D plot for performance index PI_1 ; (b) 3D plot for performance index PI_2 ; (c) condensed 2D plot for PI_1 ; (d) condensed 2D plot for PI_2 .

Figure 9. Twenty-story SAC building for numerical simulations: (a) building elevation; (b) model parameters of the lumped mass structure; (c) wireless subnet partitioning for different degrees of centralization (DC); (d) layout of semi-active hydraulic dampers (SHD) dampers on the floor plans.

Figure 10. Simulation results for the 20-story SAC structure instrumented with ideal actuators. The plots illustrate performance indexes for different sampling time steps and degrees of centralization (DC): (a) 3D plot for performance index PI_1 ; (b) 3D plot for performance index PI_2 ; (c) condensed 2D plot for PI_1 ; (d) condensed 2D plot for PI_2 .

Figure 11. Maximum inter-story drifts for cases where DC=2 with 20ms time delay and DC=4 with 40ms time delay.

Table 1. Different decentralization patterns and sampling time for the wireless and wire-based control experiments.

```

 $\mathbf{G}_{d1} = [\mathbf{0}]_{m \times q};$ 
 $s = 1;$ 
for  $i = 1, 2, \dots$ 
    Solve equation (11a) for  $\mathbf{H}_i$ ;
    Solve equation (11b) for  $\mathbf{L}_i$ ;
    Find gradient using equation (11c):  $\Delta_i = -\left(2\bar{\mathbf{B}}_d^T \mathbf{H} (\bar{\mathbf{A}}_d + \bar{\mathbf{B}}_d \mathbf{G}_d \bar{\mathbf{D}}_d) \mathbf{L} \bar{\mathbf{D}}_d^T + 2R \mathbf{G}_d \bar{\mathbf{D}}_d \mathbf{L} \bar{\mathbf{D}}_d^T\right)$ ;
    Apply shape constraint to  $\Delta_i$ ;
    iterate {
         $\mathbf{G}_{di+1} = \mathbf{G}_{di} + s \cdot \Delta_i$ ;
        Solve equation (11a) again for  $\mathbf{H}_{i+1}$  using  $\mathbf{G}_{di+1}$ ;
        if  $\text{trace}(\mathbf{H}_{i+1} \bar{\mathbf{Z}}_d) < \text{trace}(\mathbf{H}_i \bar{\mathbf{Z}}_d)$  and  $\max(|\text{eigen}(\bar{\mathbf{A}}_d + \bar{\mathbf{B}}_d \mathbf{G}_{di+1} \bar{\mathbf{D}}_d)|) < 1$ 
            exit the iterate loop;
        else
             $s = s / 2$ ;
            If ( $s < \text{machine precision}$ ), then exit the iterate loop;
        end
    };
     $s = s \times 2$ ;
    If  $\|\mathbf{G}_{di+1} - \mathbf{G}_{di}\| < \text{acceptable error}$ , then exit the for loop;
end

```

Figure. 1. Heuristic algorithm solving the coupled nonlinear matrix equations (Eq. 11a-c) for decentralized optimal time-delay output feedback control (Lunze, 1990).

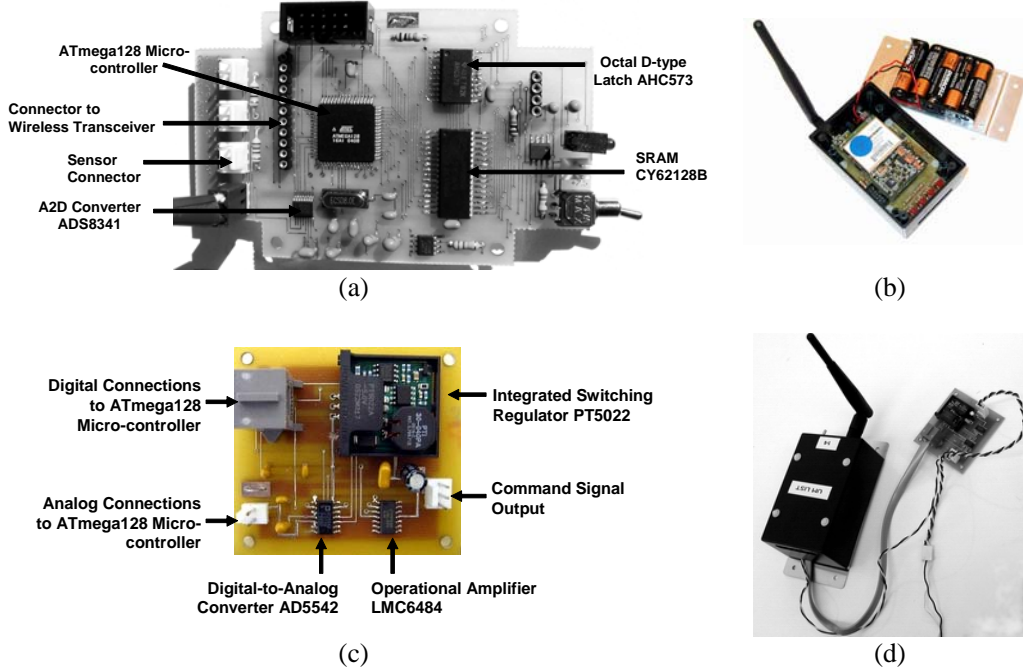


Figure 2. Overview to the prototype wireless sensing and actuation unit: (a) printed circuit board for the wireless sensing unit ($9.7 \times 5.8 \text{ cm}^2$); (b) packaged wireless sensing and control unit ($10.2 \times 6.5 \times 4.0 \text{ cm}^3$); (c) printed circuit board of the signal generation module ($5.5 \times 6.0 \text{ cm}^2$); (d) control signal module connected to wireless sensor.

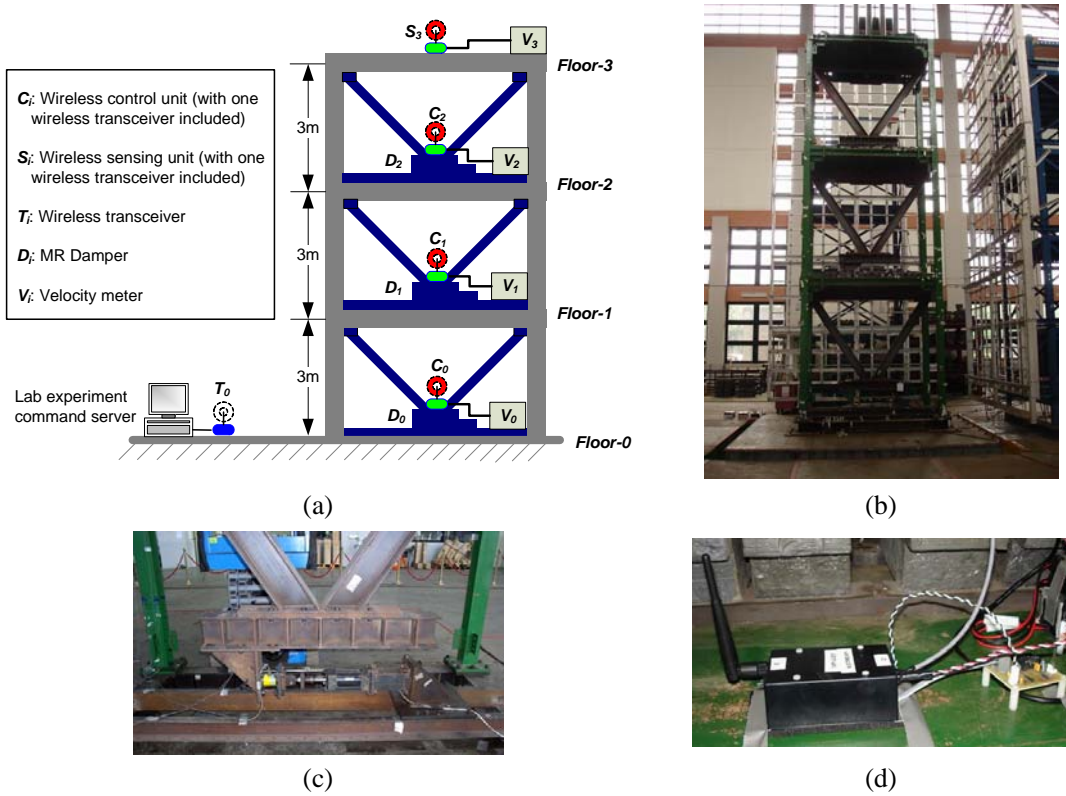


Figure 3. Laboratory setup: (a) deployment scheme of wireless sensors and actuators; (b) the 3-story test structure mounted on the shake table; (c) the MR damper installed between the 1st floor and the base floor of the structure; (d) a wireless control unit and an off-board control signal generation module.

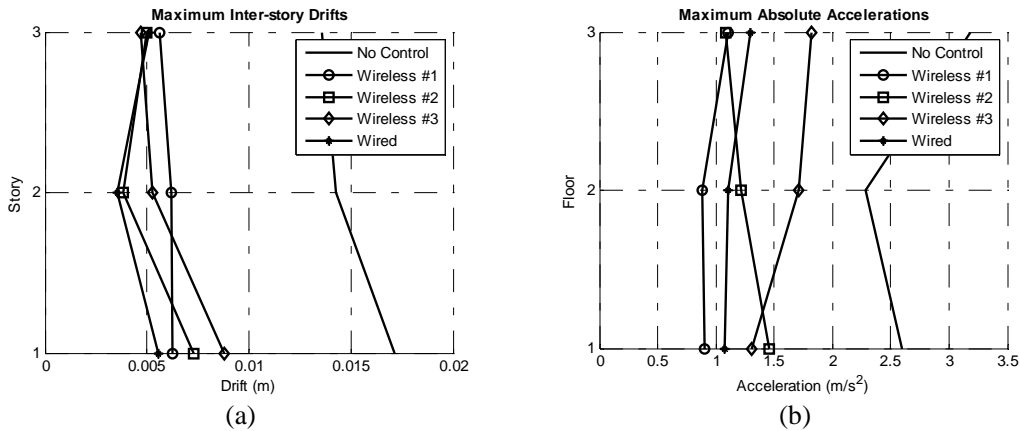


Figure 4. Experimental results of different control schemes using the El Centro excitation scaled to a peak acceleration of 1m/s^2 : (a) peak inter-story drifts; (b) peak accelerations.

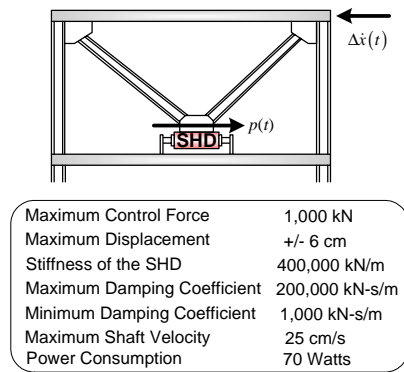


Figure 5. Key parameters of the SHD damper employed.

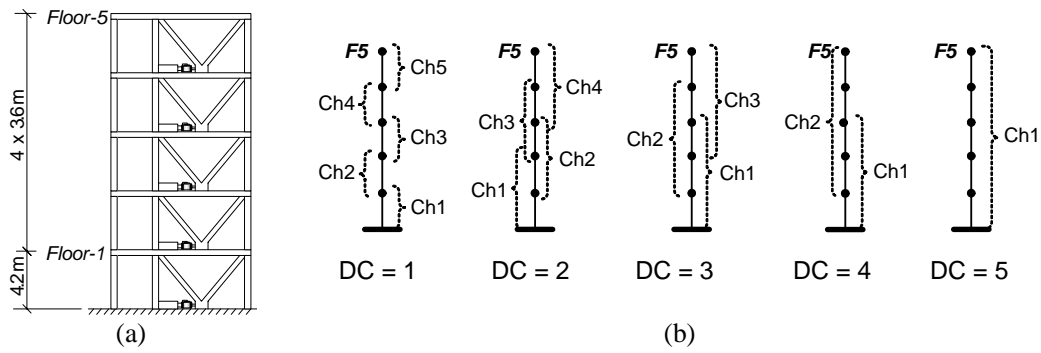


Figure 6. A five-story model similar to the Kajima-Shizuoka Building: (a) side elevation of the building; (b) information group partitioning for different degrees of centralization (DC).

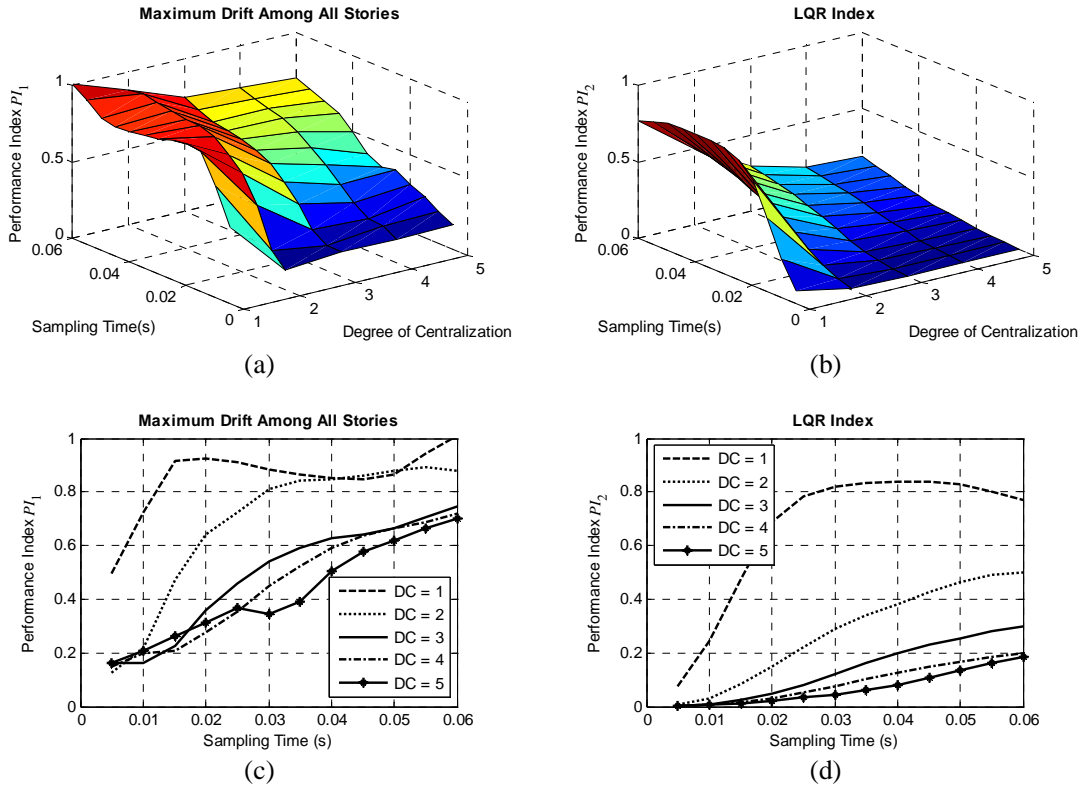


Figure 7. Simulation results for the five-story Kajima-Shizuoka Building instrumented with ideal actuators. The plots illustrate performance indexes for different sampling time steps and degrees of centralization (DC): (a) 3D plot for performance index PI_1 ; (b) 3D plot for performance index PI_2 ; (c) condensed 2D plot for PI_1 ; (d) condensed 2D plot for PI_2 .

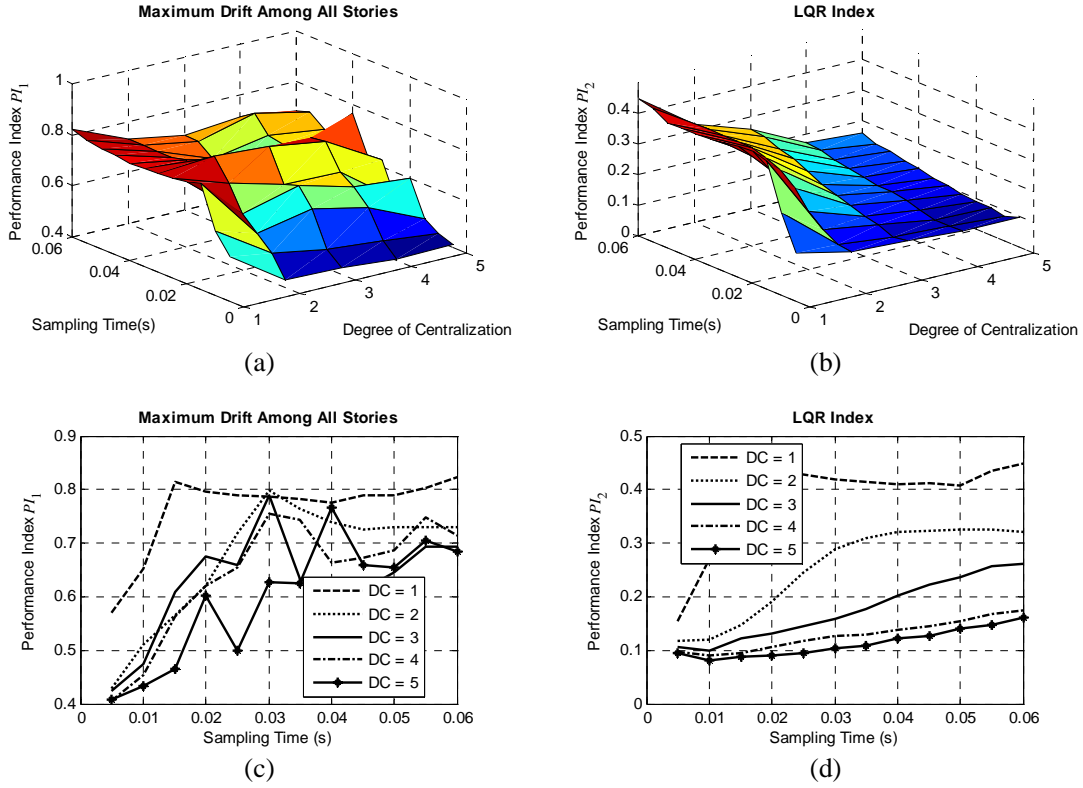


Figure 8. Simulation results for the five-story Kajima-Shizuoka Building instrumented with semi-active hydraulic dampers (SHD). The plots illustrate performance indexes for different sampling time steps and degrees of centralization (DC): (a) 3D plot for performance index PI_1 ; (b) 3D plot for performance index PI_2 ; (c) condensed 2D plot for PI_1 ; (d) condensed 2D plot for PI_2 .

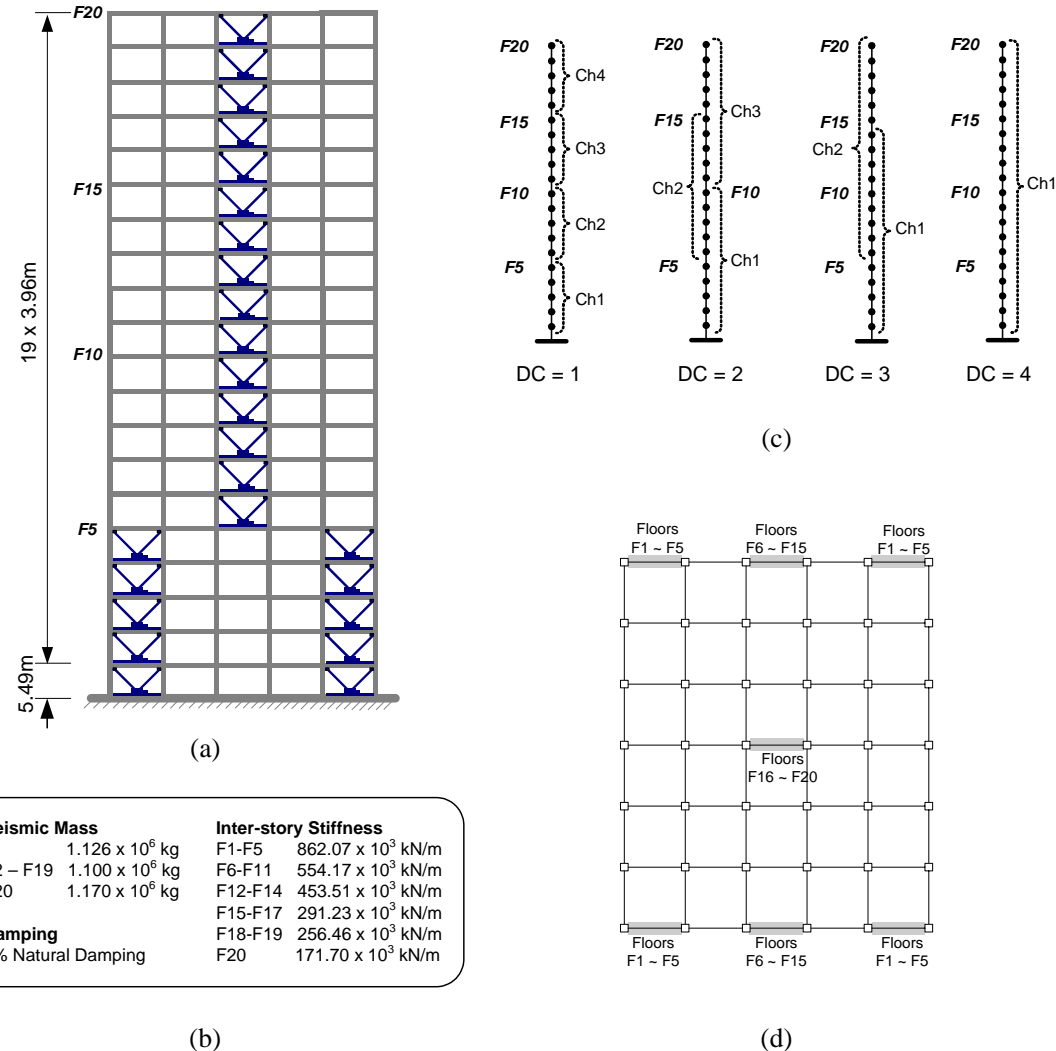


Figure. 9. Twenty-story SAC structure for numerical simulations: (a) building elevation; (b) model parameters of the lumped mass structure; (c) wireless subnet partitioning for different degrees of centralization (DC); (d) layout of semi-active hydraulic dampers (SHD) dampers on the floor plans.

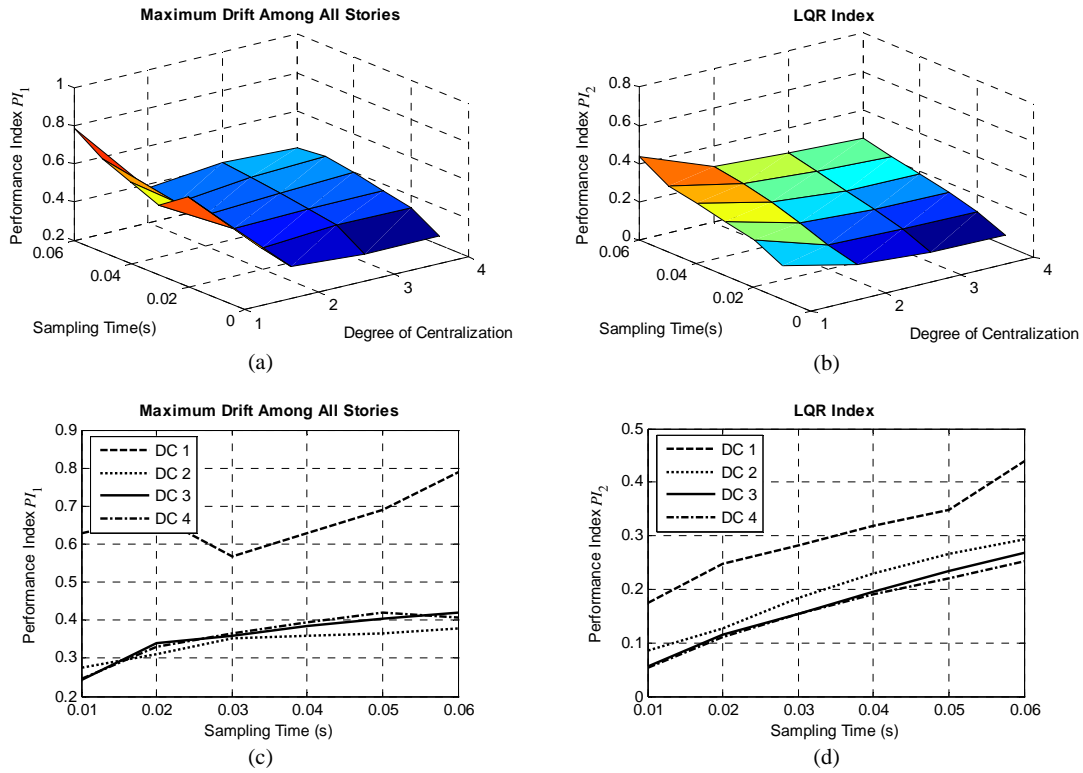


Figure 10. Simulation results for the 20-story SAC Building instrumented with ideal actuators. The plots illustrate performance indexes for different sampling time steps and degrees of centralization (DC): (a) 3D plot for performance index PI_1 ; (b) 3D plot for performance index PI_2 ; (c) condensed 2D plot for PI_1 ; (d) condensed 2D plot for PI_2 .

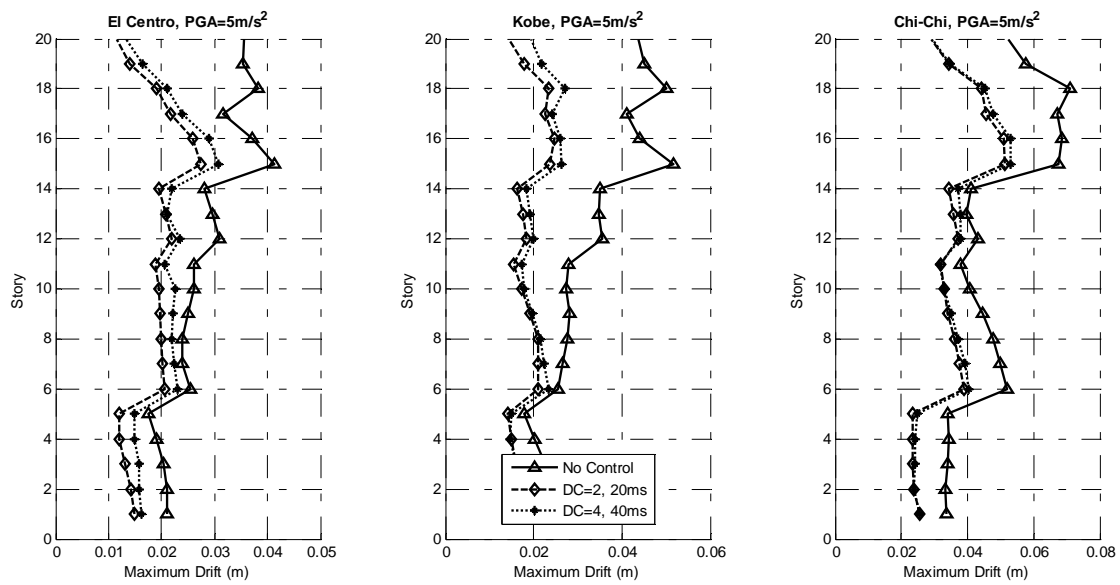


Figure. 11. Maximum inter-story drifts for cases where DC=2 with 20ms time delay and DC=4 with 40ms time delay.

Table 1. Different decentralization patterns and sampling time for the wireless and wire-based control experiments.

Degree of Centralization	Wireless System			Wired System
	1	2	3	3
Gain Matrix Pattern	\mathbf{G}_{d1} in Eq. (14)	\mathbf{G}_{d2} in Eq. (14)	\mathbf{G}_{d3} in Eq. (14)	\mathbf{G}_{d3} in Eq. (14)
Output Matrix	\mathbf{D}_{d2} in Eq. (13)	\mathbf{D}_{d2} in Eq. (13)	\mathbf{D}_{d1} in Eq. (12)	\mathbf{D}_{d1} in Eq. (12)
Sampling Time/Rate	0.02s / 50Hz	0.06s / 16.67Hz	0.08s / 12.5Hz	0.005s / 200Hz